Small-molecule inhibitor binding to an *N*-acyl-homoserine lactone synthase

Jiwoung Chung[a,1], Eunhye Goo[a,1], Sangheon Yu[a,1], Okhee Choi[a], Jeehyun Lee[a], Jinwoo Kim[b], Hongsup Kim[a], Jun Igarashi[c], Hiroaki Suga[c,d,e], Jae Sun Moon[f], Ingyu Hwang[a,2], and Sangkee Rhee[a,g,2]

[a]Department of Agricultural Biotechnology, Seoul National University, Seoul 151-921, Korea; [b]Department of Applied Biology, Gyeongsang National University, Jinju 660-701, Korea; [c]Japan Research Center for Advanced Science and Technology, University of Tokyo, Tokyo 153-8904, Japan; [d]Department of Chemistry, School of Science, University of Tokyo, Tokyo 113-0033, Japan; [e]Department of Molecular Medicine and Biopharmaceutical Sciences, Seoul National University, Seoul 151-742, Korea; [f]Plant Systems Engineering Center, Korea Research Institute of Bioscience and Biotechnology, Daejeon 305-333, Korea; and [g]Center for Fungal Pathogenesis, Seoul National University, Seoul 151-921, Korea

Edited* by Everett Peter Greenberg, University of Washington, Seattle, WA, and approved June 14, 2011 (received for review February 24, 2011)

Quorum sensing (QS) controls certain behaviors of bacteria in response to population density. In Gram-negative bacteria, QS is often mediated by *N*-acyl-L-homoserine lactones (acyl-HSLs). Because QS influences the virulence of many pathogenic bacteria, synthetic inhibitors of acyl-HSL synthases might be useful therapeutically for controlling pathogens. However, rational design of a potent QS antagonist has been thwarted by the lack of information concerning the binding interactions between acyl-HSL synthases and their ligands. In the Gram-negative bacterium *Burkholderia glumae*, QS controls virulence, motility, and protein secretion and is mediated by the binding of *N*-octanoyl-L-HSL (C8-HSL) to its cognate receptor, TofR. C8-HSL is synthesized by the acyl-HSL synthase TofI. In this study, we characterized two previously unknown QS inhibitors identified in a focused library of acyl-HSL analogs. Our functional and X-ray crystal structure analyses show that the first inhibitor, J8-C8, binds to TofI, occupying the binding site for the acyl chain of the TofI cognate substrate, acylated acyl-carrier protein. Moreover, the reaction byproduct, 5′-methylthioadenosine, independently binds to the binding site for a second substrate, *S*-adenosyl-L-methionine. Closer inspection of the mode of J8-C8 binding to TofI provides a likely molecular basis for the various substrate specificities of acyl-HSL synthases. The second inhibitor, E9C-3oxoC6, competitively inhibits C8-HSL binding to TofR. Our analysis of the binding of an inhibitor and a reaction byproduct to an acyl-HSL synthase may facilitate the design of a new class of QS-inhibiting therapeutic agents.

Quorum sensing (QS) is an intercellular signaling process that mediates certain behaviors of bacteria (including bioluminescence, biofilm formation, motility, and virulence factor production) in response to the bacterial cell population density (1–3). In Gram-negative bacteria, QS is often mediated by *N*-acyl-L-homoserine lactones (acyl-HSLs), which are synthesized by the LuxI family of acyl-HSL synthases from *S*-adenosyl-L-methionine (SAM) and acylated acyl-carrier protein (acyl-ACP), with the release of holo-ACP and 5′-methylthioadenosine (MTA) as byproducts (*SI Appendix*, Fig. S1*A*) (4, 5). Compounds of the acyl-HSL class share a homoserine lactone ring moiety, but the acyl chains conjugated to the ring via an amide bond vary in length, oxidation state at C3, and amount of saturation (*SI Appendix*, Fig. S1*A*). The recent finding that *p*-coumarate is an alternative substrate for acyl-ACP has extended the known range of possible acyl-HSL substrates (6). On the other hand, the acyl-HSL receptor is a transcriptional regulator that controls the expression of target genes in response to acyl-HSL binding (1–3).

Among the hundreds of genes regulated by QS, the most widely studied genes are those related to virulence; these genes are of particular interest because QS disruption is being investigated as a strategy for controlling virulent pathogens (7–9). QS inhibitors can act by suppressing acyl-HSL production, blocking QS receptors, or inactivating signal molecules (8–10). However, reports on the development of QS inhibitors have thus far focused only on acyl-HSL receptors (11, 12) or on enzymes involved in the SAM biosynthesis pathway (13).

We previously reported that the WT *Burkholderia glumae* strain BGR1 produces toxoflavin, a phytotoxin that acts as a key virulence factor in bacterial rice grain rot (14). In this bacterium, motility, protein secretion, and toxoflavin biosynthesis and transport are controlled by the QS signaling molecule *N*-octanoyl-L-HSL (C8-HSL). This molecule is synthesized by the acyl-HSL synthase TofI and mediates QS signaling by binding to its cognate receptor, TofR (14–16).

In the present study, we identified a TofI inhibitor, J8-C8, and a competitive inhibitor of C8-HSL binding to TofR, E9C-3oxoC6. We examined the TofI structure and the binding of J8-C8 and of MTA to TofI by X-ray crystal structure analysis of apo-TofI and a TofI/J8-C8/MTA ternary complex. These results provide an unprecedented structural view of the binding of an acyl-HSL synthase inhibitor and a reaction byproduct to an acyl-HSL synthase. Analysis of the complex suggests the molecular basis for the substrate specificity of acyl-HSL synthases toward acyl-ACPs and SAM.

Results

Identification of Two Distinct QS Inhibitors. To identify compounds that disrupt QS in *B. glumae*, we screened 55 compounds derived from previous "hits" in other Gram-negative bacterial QS systems (17). The compounds were screened by measuring the QS-mediated production of toxoflavin and C8-HSL by *B. glumae* BGR1 cells (*SI Appendix*, Fig. S2*A*). Two strong hits were identified—E9C-3oxoC6 and J8-C8—together with some minor hits (Fig. 1*A* and *SI Appendix*, Fig. S2). Both compounds diminished the production of C8-HSL and inhibited QS-dependent *ahpF* expression in BGR1 cells, but the effect of E9C-3oxoC6 was stronger (Fig. 1 *B* and *C*). In the mutant strain *B. glumae* BGS2 (*tofI*::Ω), E9C-3oxoC6 reduced toxoflavin production in the presence of 1 μM C8-HSL, but J8-C8 had no effect (Fig. 1*D*), suggesting that whereas QS inhibition by J8-C8 is mediated by TofI, E9C-3oxoC6 acts through a different mechanism. The IC_{50} values of J8-C8 and E9C-3oxoC6 for toxoflavin production were ~35 μM and 12 μM, respectively (*SI Appendix*, Fig. S3 *A* and *B*).

Author contributions: H.S., I.H., and S.R. designed research; J.C., E.G., S.Y., O.C., J.L., J.K., H.K., and J.S.M. performed research; J.I. and H.S. contributed new reagents/analytic tools; I.H. and S.R. analyzed data; and H.S., I.H., and S.R. wrote the paper.

The authors declare no conflict of interest.

*This Direct Submission article had a prearranged editor.

Data deposition: The atomic coordinates and structure factors reported in this paper have been deposited in the Protein Data Bank, www.pdb.org (PDB ID codes 3P2F and 3P2H).

[1]J.C., E.G., and S.Y. contributed equally to this work.

[2]To whom correspondence may be addressed. E-mail: ingyu@snu.ac.kr or srheesnu@snu.ac.kr.

This article contains supporting information online at www.pnas.org/lookup/suppl/doi:10.1073/pnas.1103165108/-/DCSupplemental.

MICROBIOLOGY

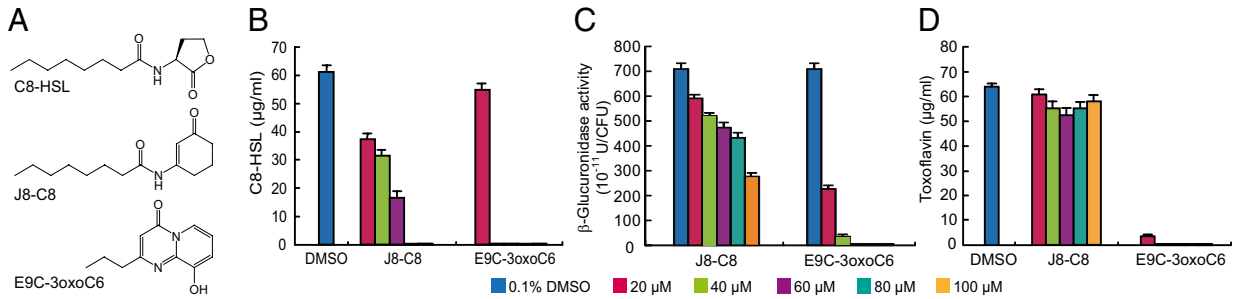

Fig. 1. Identification of small molecules that interfere with QS in *B. glumae*. (*A*) Chemical structures of C8-HSL, J8-C8, and E9C-3oxoC6. (*B*) Inhibition of C8-HSL production in *B. glumae* BGR1 cells. (*C*) Inhibition of *ahpF* expression by various concentrations of J8-C8 and E9C-3oxoC6 in BGR1 cells. (*D*) Inhibition of toxoflavin production by various concentrations of E9C-3oxoC6 in *B. glumae* BGS2 (*tofI*::Ω) cells in the presence of 1 μM C8-HSL. Error bars represent SDs from triplicate experiments.

J8-C8 Is a TofI Inhibitor. To assess our hypothesis that J8-C8 targets TofI, we measured the in vitro synthesis of C8-HSL by TofI in the presence of J8-C8 or E9C-3oxoC6. Whereas J8-C8 inhibited C8-HSL synthesis in a dose-dependent manner, E9C-3oxoC6 had no inhibitory effect on C8-HSL synthesis (Fig. 2*A*). When we then tested the effect of MTA on TofI activity, we found that 200 μM MTA inhibited TofI by ∼30% and that J8-C8 and MTA had a synergistic effect, inhibiting TofI by ∼70% when used in combination (Fig. 2*B*).

E9C-3oxoC6 Is a Competitive Inhibitor of C8-HSL Binding to TofR. To determine whether the target of E9C-3oxoC6 might be TofR, we conducted a series of competition experiments in which we measured the effect of E9C-3oxoC6 on toxoflavin production by BGS2 cells, which lack TofI. In the absence of E9C-3oxoC6, increasing the concentration of C8-HSL increased toxoflavin production in a C8-HSL concentration-dependent manner, with almost complete recovery of the WT level at 0.4 μM C8-HSL (Fig. 2*C*). Importantly, the addition of E9C-3oxoC6 at 12 μM (the IC_{50} value) delayed the recovery of toxoflavin production, but this delay was fully reversed by 0.8 μM C8-HSL (Fig. 2*C*). These results suggest that E9C-3oxoC6 competitively inhibits C8-HSL binding to TofR.

Structure of apo-TofI(3MΔ). We determined the X-ray crystal structure of TofI in its apo form using a soluble, catalytically competent TofI mutant, TofI(3MΔ). This mutant harbors three single amino acid substitutions (F42M, I149M, and L152M) and two single amino acid deletions (ΔHis91 and ΔPro92) (*SI Appendix*, Fig. S1*B* and Table S1). The crystal structure of apo-TofI(3MΔ) consists of eight β-strands and five α-helices folded into an α-β-α domain (Fig. 3*A* and *SI Appendix*, Fig. S4). Three highly disordered regions could not be modeled in the final structure of apo-TofI(3MΔ) (*SI Appendix*, Fig. S4). Structurally, these overall features in TofI are similar to those of the apo forms of two other acyl-HSL synthases, LasI (18) and EsaI (19), with an rmsd of 1.4 Å (164 Cα atoms) and 2.2 Å (139 Cα atoms), respectively (*SI Appendix*, Fig. S5). Notable differences in the *N*-terminal region were seen among the three structures.

As noted previously (18, 19), an apparent pocket exists on the concave side of the β-sheet; this pocket is located primarily between β4 and β5; is enclosed by three helices, α1, α3, and α4; and is oriented parallel to the β-sheet (Fig. 3*A*). In a structure of apo-TofI(3MΔ), five water molecules are clustered at the entrance to the pocket via direct or water-mediated hydrogen bonding to the side chain of Arg104 and the main-chain carbonyl oxygen of Phe105 (*SI Appendix*, Fig. S6*A*), leaving the inside of the pocket vacant.

J8-C8 Binding Mode in the TofI(3MΔ)/J8-C8/MTA Ternary Complex. The crystal structure of the TofI(3MΔ)/J8-C8/MTA ternary complex shows the binding of J8-C8 and MTA to TofI(3MΔ) and the structural stabilization of the segment Gly32–Glu40, which is highly disordered in the apo form (Figs. 3*B* and 4*A* and *SI Appendix*, Fig. S6*C*). This segment forms part of the loop between α1 and β2 (*SI Appendix*, Fig. S4). The structure of TofI(3MΔ) in the ternary complex is essentially identical to that in the apo form (rmsd of 0.23 Å for 175 Cα atoms), except for the ordering of the α1–β2 loop residues.

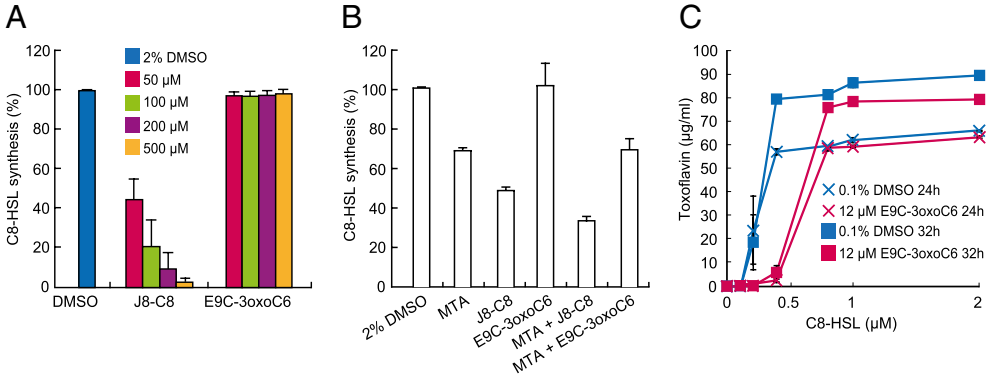

Fig. 2. Molecular mechanisms of J8-C8 and E9C-3oxoC6 inhibitory activity. (*A*) Inhibition of C8-HSL synthesis by J8-C8 in BGR1 cells. (*B*) Inhibition of C8-HSL synthesis by MTA and synergistic inhibitory effect of J8-C8. The amount of C8-HSL produced for each treatment is shown relative to that produced for DMSO treatment alone (100%). (*C*) Toxoflavin inhibition in BGS2 cells in the presence of 12 μM E9C-3oxoC6 is relieved by increasing amounts of C8-HSL. Levels of toxoflavin production were measured in the presence of 12 μM E9C-3oxoC6 or 0.1% DMSO at 24 h and 32 h after the addition of C8-HSL. Error bars represent SDs from triplicate experiments.

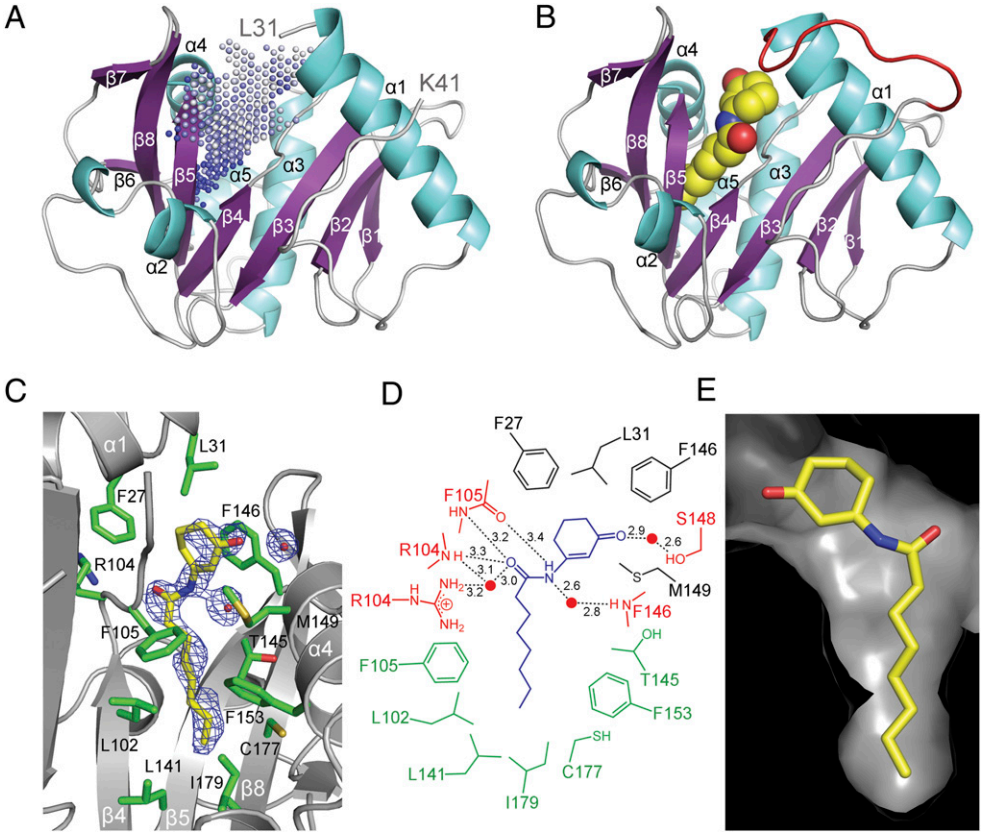

Fig. 3. Structure of TofI and the binding site of J8-C8. (*A*) The overall structure of apo-TofI(3MΔ) is shown with the putative pocket region, as defined by the program PocketPicker (23), indicated by dots. (*B*) The TofI(3MΔ)/J8-C8/MTA ternary complex is presented in an orientation identical to that in *A*. The bound J8-C8 is shown as a space-filling model, and the stabilized loop residues between α1 and β2 are shown in red. For clarity, a bound MTA in the ternary complex is not shown. (*C*) The J8-C8 binding site in the ternary complex is displayed with its neighboring residues and with the $2F_o$–F_c electron density map (contoured at 0.9σ) for J8-C8. (*D*) Schematic diagram of the interactions between TofI(3MΔ) and J8-C8 in the ternary complex. Enzyme residues involved in direct hydrogen bonds are indicated in red with interatomic distances (Å). Residues involved in van der Waals interactions within 4.0 Å of the acyl chain or ring moiety of J8-C8 are shown in green and black, respectively. A water molecule is indicated with a red circle. (*E*) The pocket-shaped binding site of J8-C8 in the ternary complex is shown as a surface model. This view is rotated by ~180° from that shown in *C*.

In the ternary complex, J8-C8 is bound to the pocket observed in the apo-TofI(3MΔ) structure. The octanoyl chain is almost in an elongated conformation (Fig. 3*C* and *SI Appendix*, Fig. S6*B*) and is surrounded by hydrophobic residues of β4 (Leu102 and Phe105), β5 (Thr145 and Phe146), α4 [Met149 (Ile149 in the WT enzyme) and Phe153], and α1 (Phe27 and Leu31). The innermost part of the pocket is sealed off by a layer of residues that includes Leu141, Cys177, and Ile179. Compared with the apo structure, no significant positional changes occur in the main and side chains of residues in the vicinity of the pocket, indicating that the pocket remains in a highly static mode. Specifically, different conformations of the side chains, which are defined with the ordered electron density, were found in the pocket for Thr145 and Leu102 (*SI Appendix*, Fig. S6 *A* and *B*), but these minor changes, with displacement of ~1.2 Å, had no significant effect on the size and shape of the pocket. The partially disordered ring moiety in J8-C8 (*SI Appendix*, Fig. S7) is likely stabilized by stacking interactions with Phe146 at a distance of 3.9 Å, as well as by van der Waals interactions with Phe27 and Leu31. In addition, the carbonyl oxygen on the ring faces toward the *N*-terminal end of helix α4 with the positive end of the helix dipole and is within hydrogen-bonding distance to a water molecule that forms a hydrogen bond at a distance of 2.6 Å to Ser148 (Fig. 3*D*). The amide bond of the inhibitor appears to make several hydrogen bonds with residues in the binding site. Specifically, the nitrogen and carbonyl oxygen in the amide bond are within hydrogen-bonding distance of the main chain atoms of Phe105 (3.2–3.4 Å) and Arg104 (3.3 Å), and of water molecules (2.6–3.0 Å) that might form a hydrogen-bonding network with the nearby residues Arg104 and Phe146. J8-C8 is almost buried in the pocket, such that only ~6% (33 $Å^2$) of the possible surface area is exposed. The ring moiety of J8-C8 constitutes most of the exposed area, suggesting that the hydrophobicity of the octanoyl chain is a major driving force in stabilizing the binding of J8-C8 to TofI(3MΔ). The dissociation constants for J8-C8 with TofI variants in solution were in the range of 3.6–4.1 μM, as determined by fluorescence titration (*SI Appendix*, Fig. S8).

MTA Binding Mode in the TofI(3MΔ)/J8-C8/MTA Ternary Complex. Unlike the J8-C8 inhibitor bound to the concave side of the β-sheet, the reaction byproduct MTA is bound to the convex side of the β-sheet, which is surrounded by helix α1, a long loop between α1 and β2 (including the newly stabilized segment Gly32–Glu40), α2, and β7 (Fig. 4*A*). In the tertiary complex, MTA remains partially exposed to solvent, with a solvent-exposed surface area of 92 $Å^2$. Its binding site is separated from the amide bond of J8-C8 by ~8.0 Å, with intervention by the bulky side chains of Phe146 and Trp33 (Fig. 4 *A* and *B*). The adenine moiety of MTA forms several hydrogen bonds at distances of 2.6–3.2 Å with the side chains of residues Asp45, Gln46, and Arg104, as well as hydrophobic interactions with Leu78, Val82, and Phe83 (Fig. 4 *C* and *D*). In addition to these interactions, the 5′-methylthioribose ring of MTA mediates a face-to-face stacking interaction with the side chain of Trp33 within 3.5–3.9 Å. It

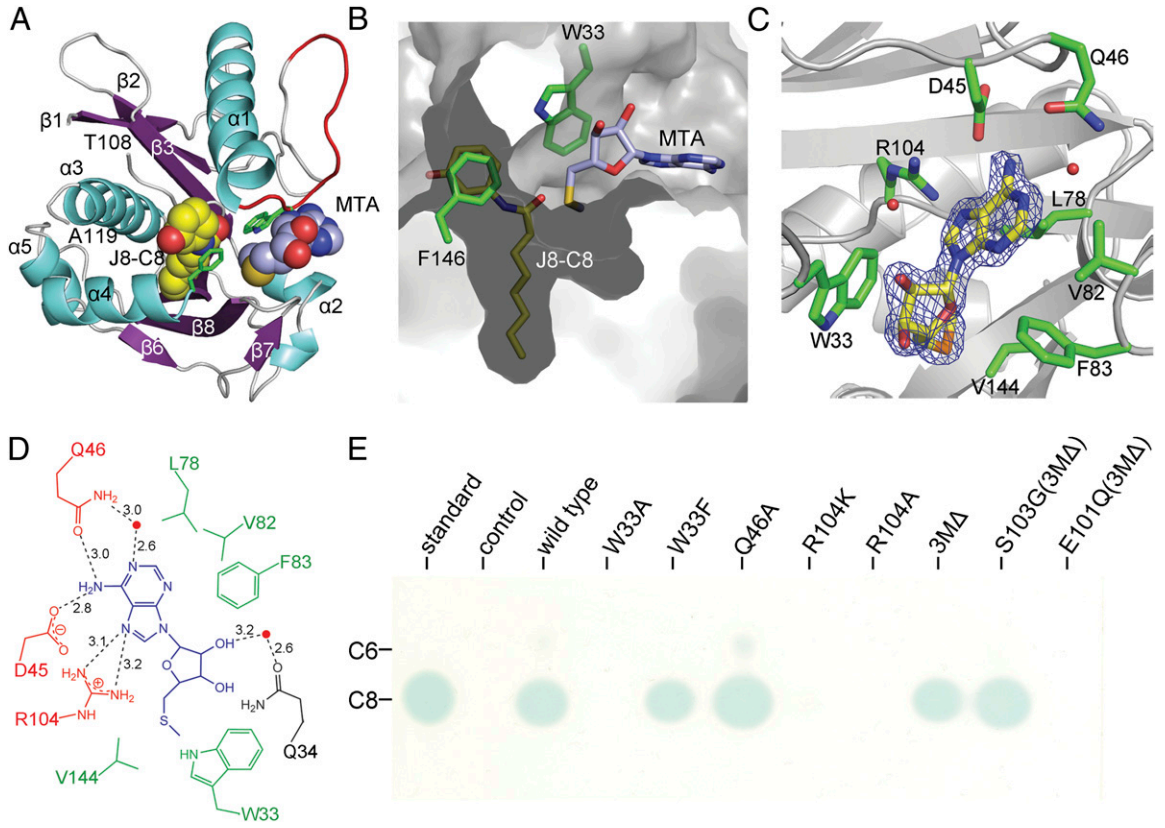

Fig. 4. Structural and functional features of the ternary complex. (*A*) The overall structure of the ternary complex. J8-C8 and MTA are represented by space-filling models, and the stabilized loop residues between α1 and β2 are shown in red. (*B*) Close-up molecular surface representation of the J8-C8 and MTA binding sites separated by Phe146 and Trp33. (*C*) Close-up view of the MTA-binding region and the nearby interacting residues. The F_o–F_c electron density map for MTA is contoured at 3.5σ. (*D*) Schematic diagram of the interactions between bound MTA and residues in its binding site. Residues participating in hydrogen bonds (red) and in van der Waals interactions (green) are shown. (*E*) Detection of acyl-HSLs produced by various TofI enzymes. Unlike the other enzymes, the S103G and E101Q mutants contain additional mutations shown in TofI(3MΔ) to express the mutant protein as a soluble form. Details of the thin-layer chromatographic analysis are provided in *SI Appendix*, Fig. S1*B*.

forms a hydrophobic interaction with Val144, whereas the hydroxyl group at C2′ of the ribose ring forms a water-mediated hydrogen bond with Gln34.

Notably, residues Trp33, Asp45, and Arg104 are strictly conserved among members of the LuxI-type acyl-HSL synthase family (*SI Appendix*, Fig. S4). In a functional analysis, we found that the aromaticity of Trp33 is essential for C8-HSL production (Fig. 4*E*). Specifically, the W33F mutant, which maintains a stacking interaction with the MTA 5′-methylthioribose ring, was catalytically active. The R104K and R104A mutants were catalytically inactive, suggesting the functional significance of the arginine side chain in a hydrogen-bonding network (directly with the adenine moiety of MTA and via a water-mediated interaction with J8-C8) (Figs. 3*D* and 4*D*). These observations are consistent with a previous mutational analysis of an acyl-HSL synthase RhlI (20). As for Asp45, our mutant enzymes, such as D45N and D45A, were not expressed successfully as a soluble form, although a functional study of EsaI indicated that this conserved aspartate is crucial for activity (19). Given that the side chains of the MTA-interacting residues, with the exception of those in the Gly32–Glu40 loop, maintained identical orientations between the apo and ternary structures in this study, the stabilization of residues Gly32–Glu40, particularly Trp33, appears to be a major impetus for the binding of MTA.

Discussion

The binding of several QS inhibitors to acyl-HSL receptors has been characterized in detail (12), but their putative competition with acyl-HSLs for binding to their cognate receptors has not been demonstrated previously. To the best of our knowledge, our competition experiments provide previously undescribed biochemical evidence of the competitive behavior of E9C-3oxoC6 toward TofR binding. This approach may be beneficial for validating the competition between other QS inhibitors and cognate acyl-HSLs for binding to proteins of the LuxR family.

One of the compounds identified in this study, J8-C8, is a structural analog of the TofI product C8-HSL and is the previously unidentified inhibitor of a LuxI-type acyl-HSL synthase. Thus far, acyl-HSL synthase structural information has been limited to the apo forms of LasI (18) and EsaI (19). Thus, our crystallographic analysis of a TofI/J8-C8/MTA ternary complex provides unprecedented molecular details of the binding interactions between an acyl-HSL inhibitor and an acyl-HSL synthase, and suggests the molecular basis for the selectivity of TofI for octanoyl-ACP from among the pool of acyl-ACPs presumed to be present during catalysis. Consistent with these functional features, the size of the pocket in TofI is highly specific for the octanoyl chain (Fig. 3*E*), and J8-C6, which differs from J8-C8 only in its hexanoyl chain, failed to disrupt QS in *B. glumae* in our experiments (*SI Appendix*, Fig. S2*A*), possibly because of its poor binding to TofI (*SI Appendix*, Fig. S8*D*). These structural considerations suggest that J8-C8 acts as a competitive inhibitor of the octanoyl-ACP substrate.

The TofI reaction scheme (*SI Appendix*, Fig. S1*A*) indicates that the MTA-binding site characterized in the TofI ternary complex is the binding site for SAM, a substrate common to all acyl-HSL

synthases. Many of the MTA-interacting residues are highly or strictly conserved in the acyl-HSL synthase family (*SI Appendix*, Fig. S4); thus, this common substrate can be accommodated by all members of this family. In the ternary complex, the binding sites for J8-C8 and MTA are ~8.0 Å apart and are separated primarily by Phe146 and Trp33 (Fig. 4*B*). Behind these residues, a channel leading toward the interior of the enzyme is large enough to accommodate the methionine moiety of SAM and to connect the inhibitor- and MTA-binding sites (*SI Appendix*, Fig. S10*A*). Thus, reactions for acylation and lactonization could occur in this region on binding of octanoyl-ACP and SAM.

A previous kinetic analysis of an acyl-HSL synthase, RhlI, suggested that the ionizing residue plays a part in the acylation reaction that leads to deprotonation of the α-amino group of SAM and subsequent nucleophilic attacks on the thioester bond of acyl-ACP (21). After acylation, lactonization appears to proceed via a direct attack of the carboxylate oxygen on the methylene carbon adjacent to the sulfonium ion within an *N*-acyl–SAM intermediate (21). In particular, various experiments consistently indicated that this lactonization step does not require a general acid-base catalysis (21). Thus, formation of acyl-HSL depends on the presence of a catalytic base. In previous structural and functional analyses of EsaI (19), a water molecule that can be activated by enzyme residue(s) in a hydrogen-bonding network has been suggested as the possible catalytic base in the acylation reaction. Catalytic features similar to this proposition were also characterized in the modeled structure for a TofI(3MΔ)/J8-C8/SAM complex (*SI Appendix*, Fig. S9). No obvious residues exist to act as a catalytic base near the amide bond of J8-C8, presumably mimicking the thioester bond of acyl-ACP, except for two water molecules. In fact, Glu101 and Ser103, which are conserved in the LuxI family of acyl-HSL synthases (*SI Appendix*, Fig. S4) (20), are the only possible candidates that could activate a water molecule via a hydrogen-bonding network, although the side chain of Glu101 appears to be in a more favorable orientation for the proposed role compared with that of Ser103, which faces away from a water molecule (*SI Appendix*, Fig. S9). Mutation of the corresponding glutamate residue, Glu97 in EsaI (19) and Glu101 in RhlI (20), nearly abolished enzyme activity. In EsaI, mutation of the serine residue corresponding to Ser103 in TofI also inactivated the enzyme (19); however, in our study, the S103G mutant enzyme, with additional mutations in TofI(3MΔ), retained enzyme activity almost comparable to that of TofI(3MΔ) (Fig. 4*E*). Our functional analysis of the E101Q mutant indicated that Glu101 is important for catalytic activity (Fig. 4*E*). Taken together, these structural and functional data support a water molecule as a catalytic base that is activated via a hydrogen-bonding network with Glu101. Nonetheless, we cannot rule out an alternative possibility, that conformational changes induced by the binding of SAM and/or acyl-ACP could properly juxtapose a possible catalytic base into the α-amino group of SAM. The observed perturbation of the p*K* value for the ionizing residue on binding of acyl-ACP suggests those conformational changes (21), which could not be identified in our ternary structure lacking the ACP moiety. In fact, different conformations of the *N*-terminal region, which corresponds to the MTA-binding site in TofI, were characterized among acyl-HSL synthases, even in the absence of ligand (*SI Appendix*, Fig. S5), implying that this particular region has a dynamic feature for catalysis (18). Further investigation is needed to resolve the mechanism of the acylation reaction.

Unlike the MTA-binding site, the inhibitor-binding pocket of acyl-HSL synthases exhibits sequence variations that alter its size and shape. The pocket-forming residues have relatively well-conserved hydrophobic features, but are not identical (*SI Appendix*, Fig. S4 and Table S2). Close inspection of the corresponding pocket regions in the apo forms of LasI (18) and EsaI (19) reveals sequence variations in and near the pocket area, as well as localized structural differences in α3 and α4, leading to different shapes and sizes of the pocket (*SI Appendix*, Fig. S10). These changes are consistent with the previously proposed tunnel- and pocket-shaped binding sites for the 3-oxo-C12 acyl chains in LasI and the 3-oxo-C6 acyl chains in EsaI (19). Thus, the specificity of acyl-HSL synthases for their cognate acyl-ACPs is likely achieved through sequence variations in the pocket.

Our structural and functional analysis showing that the inhibitor J8-C8 occupies the binding site for the acyl chain of acyl-ACP suggests the molecular basis for the acyl chain-length specificity of acyl-HSL synthases and the binding of MTA. Compounds mimicking J8-C8 with variations in acyl chain length would be candidates for narrow-range, rather than wide-spectrum, therapeutic agents. This structural information is expected to serve as a basis for fragment-based design of a new class of QS inhibitors that act against acyl-HSL synthases. In particular, we speculate that a compound containing both J8-C8 and MTA moieties would be a potent and broad-spectrum agent against various QS-dependent pathogens, including those affecting humans.

Materials and Methods

Acyl-HSL and Toxoflavin Production Assays. Assays for production of QS signaling molecules (22) and toxoflavin (14) were performed as described previously. Toxoflavin was kindly provided by Dr. Tomohisa Nagamatsu, Okayama University, Okayama, Japan.

Crystallization and Structure Determination. All TofI variants used in this study were constructed using the full-length *tofI* gene as a template for PCR carried out with sequence-specific or mutagenic primers (*SI Appendix*, Table S4). The resulting TofI variants were expressed in *Escherichia coli* strain BL21(DE3) pLysS (Novagen). For crystallization, the TofI(3MΔ) mutant was purified by ion-exchange and size-exclusion chromatography. Single-wavelength data for the apo-TofI(3MΔ) and its ternary complexes were obtained to 2.3 Å and 2.0 Å resolution, respectively, on beamlines 4A and 6C at the Pohang Accelerator Laboratory, Pohang, Korea. Structures were solved by molecular replacement and refined to final R_{work}/R_{free} values of 22.9/27.0% for the apo form and 20.0/23.1% for its ternary complex. For functional assays, enzymes with C-terminal His-tags were purified by immobilized metal-affinity chromatography.

Fluorescence Measurements. The binding of J8-C8 or J8-C6 to TofI variants was followed using steady-state fluorescence measurements at 25 °C. Ligand binding was measured by following the change in the intrinsic fluorescence of TofI(Δ) or TofI(3MΔ) as a function of ligand concentration. The excitation and emission wavelengths were 280 nm and 350 nm, respectively.

ACKNOWLEDGMENTS. We thank Dr. Takashi Ooi for the X-ray crystal structure analysis of E9C-3oxoC6. Funding for this work was provided by the Crop Functional Genomics Center and National Research Foundation Grants R11-2008-062-01002-0 and 2010-0025883 (to S.R.) of the Korean Ministry of Education, Science, and Technology; Creative Research Initiatives Programs of the National Research Foundation Grant 2010-0018280 (to I.H.), and World Class University Project of the Ministry of Education, Science and Technology and the National Research Foundation Grant R31-2008-000-10103-0 (to H.S.). H.S. also was supported by the Japan Science and Technology Innovative Technology Development Fund and Otsuka Chemical Corporation, Ltd.

1. Fuqua C, Greenberg EP (2002) Listening in on bacteria: Acyl-homoserine lactone signaling. *Nat Rev Mol Cell Biol* 3:685–695.
2. Waters CM, Bassler BL (2005) Quorum sensing: Cell-to-cell communication in bacteria. *Annu Rev Cell Dev Biol* 21:319–346.
3. Parker CT, Sperandio V (2009) Cell-to-cell signaling during pathogenesis. *Cell Microbiol* 11:363–369.
4. Schaefer AL, Val DL, Hanzelka BL, Cronan JE, Jr., Greenberg EP (1996) Generation of cell-to-cell signals in quorum sensing: Acyl homoserine lactone synthase activity of a purified *Vibrio fischeri* LuxI protein. *Proc Natl Acad Sci USA* 93:9505–9509.
5. Moré MI, et al. (1996) Enzymatic synthesis of a quorum-sensing autoinducer through use of defined substrates. *Science* 272:1655–1658.
6. Schaefer AL, et al. (2008) A new class of homoserine lactone quorum-sensing signals. *Nature* 454:595–599.
7. Rasko DA, Sperandio V (2010) Anti-virulence strategies to combat bacteria-mediated disease. *Nat Rev Drug Discov* 9:117–128.

8. Hentzer M, et al. (2003) Attenuation of *Pseudomonas aeruginosa* virulence by quorum-sensing inhibitors. *EMBO J* 22:3803–3815.
9. Smith RS, Iglewski BH (2003) *Pseudomonas aeruginosa* quorum sensing as a potential antimicrobial target. *J Clin Invest* 112:1460–1465.
10. Dong YH, et al. (2001) Quenching quorum-sensing–dependent bacterial infection by an *N*-acyl homoserine lactonase. *Nature* 411:813–817.
11. Rasmussen TB, Givskov M (2006) Quorum-sensing inhibitors: A bargain of effects. *Microbiology* 152:895–904.
12. Zou Y, Nair SK (2009) Molecular basis for the recognition of structurally distinct autoinducer mimics by the *Pseudomonas aeruginosa* LasR quorum-sensing signaling receptor. *Chem Biol* 16:961–970.
13. Gutierrez JA, et al. (2009) Transition state analogs of 5′-methylthioadenosine nucleosidase disrupt quorum sensing. *Nat Chem Biol* 5:251–257.
14. Kim J, et al. (2004) Quorum sensing and the LysR-type transcriptional activator ToxR regulate toxoflavin biosynthesis and transport in *Burkholderia glumae*. *Mol Microbiol* 54:921–934.
15. Kim J, et al. (2007) Regulation of polar flagellum genes is mediated by quorum sensing and FlhDC in *Burkholderia glumae*. *Mol Microbiol* 64:165–179.
16. Goo E, Kang Y, Kim H, Hwang I (2010) Proteomic analysis of quorum-sensing–dependent proteins in *Burkholderia glumae*. *J Proteome Res* 9:3184–3199.
17. Smith KM, Bu Y, Suga H (2003) Library screening for synthetic agonists and antagonists of a *Pseudomonas aeruginosa* autoinducer. *Chem Biol* 10:563–571.
18. Gould TA, Schweizer HP, Churchill ME (2004) Structure of the *Pseudomonas aeruginosa* acyl-homoserinelactone synthase LasI. *Mol Microbiol* 53:1135–1146.
19. Watson WT, Minogue TD, Val DL, von Bodman SB, Churchill ME (2002) Structural basis and specificity of acyl-homoserine lactone signal production in bacterial quorum sensing. *Mol Cell* 9:685–694.
20. Parsek MR, Schaefer AL, Greenberg EP (1997) Analysis of random and site-directed mutations in *rhlI*, a *Pseudomonas aeruginosa* gene encoding an acylhomoserine lactone synthase. *Mol Microbiol* 26:301–310.
21. Raychaudhuri A, Jerga A, Tipton PA (2005) Chemical mechanism and substrate specificity of RhlI, an acylhomoserine lactone synthase from *Pseudomonas aeruginosa*. *Biochemistry* 44:2974–2981.
22. Shaw PD, et al. (1997) Detecting and characterizing *N*-acyl-homoserine lactone signal molecules by thin-layer chromatography. *Proc Natl Acad Sci USA* 94:6036–6041.
23. Weisel M, Proschak E, Schneider G (2007) PocketPicker: Analysis of ligand binding-sites with shape descriptors. *Chem Cent J* 1:7, doi:10.1186/1752-153X-1-7.